*Aerosol and Air Quality Research*, 18: 2997–3008, 2018

ISSN: 1680-8584 print / 2071-1409 online
doi: 10.4209/aaqr.2018.04.0123

# Size Distributions of Water-Soluble Inorganic Ions in Atmospheric Aerosols during the Meiyu Period on the North Shore of Taihu Lake, China

**Duanyang Liu[1,2*], Yan Su[3], Huaqing Peng[3], Wenlian Yan[1,2], Yi Li[4], Xuejun Liu[5], Bin Zhu[6], Honglei Wang[6], Xiliang Zhang[7]**

[1] *Key Laboratory of Transportation Meteorology, China Meteorological Administration, Nanjing 210008, China*
[2] *Meteorological Observatory of Jiangsu Province, Nanjing 210008, China*
[3] *Meteorological observatory of Wuxi in Jiangsu Province, Wuxi 214101, China*
[4] *Department of Atmospheric Science, Colorado State University, Fort Collins, CO 80523, USA*
[5] *College of Resources and Environmental Sciences, China Agricultural University, Beijing 100193, China*
[6] *Key Laboratory for Atmospheric Physics and Environment CMA, Nanjing University of Information Science and Technology, Nanjing 210044, China*
[7] *Huzhou Meteorological observatory of Zhejiang Province, Huzhou 313000, China*

## ABSTRACT

In order to research the impact on air pollution from Meiyu (a special period of seasonal heavy rainfall between late May and June in the middle-lower Yangtze area in China (Qian *et al.*, 2009)), the pollutant gas concentrations, size distributions, and water-soluble inorganic ions of aerosols were measured on the north shore of Taihu Lake from June 10 to June 26, 2014. Results show that the $PM_{1.1}$ (aerodynamic diameter ≤ 1.1 μm) grew in particle size, becoming $PM_{1.1\text{-}2.1}$ (1.1 μm ≤ aerodynamic diameter ≤ 2.1 μm) and then CPM (coarse particle matter; aerodynamic diameter > 2.1 μg) due to coagulation growth and chemical reactions, prior to Meiyu. The ions, anions, and cations all exhibited bimodal distributions before Meiyu, with peak positions of 0.43–1.1 and 9–10 μm, and trimodal distributions during Meiyu, with unfixed peak positions. The spectral size distributions of the $SO_4^{2-}$, $NO_3^-$, and $NH_4^+$ were all bimodal or trimodal before Meiyu, and SNA ($SO_4^{2-}$, $NO_3^-$, and $NH_4^+$) was the main component of the $PM_{1.1}$ and $PM_{1.1\text{-}2.1}$. Vehicle emissions were more important and the secondary formation of $SO_4^{2-}$ from $SO_2$ occurred more readily during Meiyu than before Meiyu. The nitrogen oxidation ratio (NOR) was lower than the sulfur oxidation ratio (SOR), and the secondary formation of $NO_3^-$ from $NO_x$ infrequently occurred in Wuxi compared to that of $SO_4^{2-}$ from $SO_2$. The samples collected during the pre-Meiyu season and Meiyu all fell below the line 1:1 (CE:AE) (cation equivalence:anion equivalence), suggesting that the volatilization of ammonium and nitrate as well as unmeasured hydrogen ions may have caused the loss of cations, which resulted in insufficient cations for neutralizing the anions and subsequently, acidic properties for the aerosol. [$NH_4^+$ + $Ca^{2+}$] are evidently sufficient for neutralizing [$SO_4^{2-}$ + $NO_3^-$ + $NO_2^-$ + $Cl^-$].

***Keywords:*** Fine particles; Size distribution; Water-soluble inorganic ions; Meiyu; Taihu Lake.

## INTRODUCTION

Particulate matter (PM), i.e., $PM_{10}$ (aerodynamic diameter ≤ 10 μm) and $PM_{2.5}$ (aerodynamic diameter ≤ 2.5 μm), has drawn more and more attentions in recent years since its important roles in human health effects, atmospheric processes and even global climate change (Bisht *et al.*, 2015; Liu *et al.*, 2016b; Zhou *et al.*, 2016).

Compared to developed countries, emerging and developing countries are facing more serious PM pollution and much more complex PM sources (Ram *et al.*, 2012; Li *et al.*, 2014; Shi *et al.*, 2016; Xu *et al.*, 2016). With the rapid industrialization and urbanization sustained in China, fossil fuel (esp. coal and petroleum) combustion (including industrial emission and vehicle exhaust) produced a large amount of coarse aerosols, along with secondary fine particles or aerosols, causing an urgent air pollution problem (Huang *et al.*, 2006; Cheng *et al.*, 2012; Zhou *et al.*, 2016; Li *et al.*, 2018). It is true especially in the fast-developing regions, such as the Pearl River Delta (PRD) region (Zhao *et al.*, 2014), the North China Plain (NCP) (Gao *et al.*, 2016; Huang *et al.*, 2016; Jiang *et al.*, 2017; Liu *et al.*, 2016a; Ma *et al.*, 2016; Su *et al.*, 2018), and the Yangtze River Delta (YRD) region (Wang *et al.*, 2012b; Ding *et al.*, 2013; Wang *et al.*, 2014; Liang *et al.*, 2017).

* Corresponding author.
*E-mail address:* liuduanyang2001@126.com

The $PM_{10}$ have been measured on a national scale at the routine observation stations set by MEP (Ministry of Environmental Protection of China), and the $PM_{2.5}$ data were partly available since the beginning of 2012. However, these measurements are mostly concentrated on the mass concentrations rather than the PM chemical species. The PM chemical species research is useful not only for exploring the adverse health effects evocators but for identifying emission sources which are compulsive information for efficient mitigation strategies (Zhou *et al.*, 2016). Some studies also investigated the size distribution of the aerosol chemical compositions in Beijing (Yang *et al.*, 2015; Liu *et al.*, 2016c; Tan *et al.*, 2016; Su *et al.*, 2018). Until now, the PM chemical species investigations have been carried out by some researchers in the YRD region (e.g., Zhao *et al.*, 2015), in different seasons including spring and summer (Du *et al.*, 2011; Wen *et al.*, 2013), autumn and winter (Yang *et al.*, 2012; Wen *et al.*, 2014; Wang *et al.*, 2015, 2016). And some other studies were also conducted about the effect of crop-straw burning on PM pollution (Wang *et al.*, 2012a). However, the precipitation influence on the size distributions and water-soluble inorganic ions of PM has seldom been studied to date.

Wuxi, as a booming economic metropolis, is in the center of Yangtze River Delta Cities Group Area (YRDCGA) region, near the Tai Lake. It is usually downwind for the entire YRDCGA, and even the NCP's prevailing winds are between north and northwest. Meanwhile, it is also the receptor site of the winter atmospheric pollution and the upwind site of YRDCGA in the summertime (Guo *et al.*, 2013; Peng *et al.*, 2016). How the fine particles increase to the coarse particles, what are the ions' spectral distributions and what are the main components of the particles during the Meiyu period? These are important questions for us. Therefore, the PM features in Wuxi are essential to understanding the pollution of PM caused by the local and intensive emissions in YRDCGA, and helpful to understand thoroughly the atmospheric pollution regional transport within the YRDCGA. The present study aims to fill this gap through examining the size distributions and water-soluble inorganic ions of aerosol before and during the Meiyu period in June 2014.

## INSTRUMENTS AND EXPERIMENTS

### *Observation Station*

All the measurements were conducted on June 10–26, 2014, at the monitoring site in Wuxi meteorological observational station (WMOS, 31.6127°N, 120.3544°E, altitude: 3.2 m), which is located in the northeast of Wuxi (Fig. 1), China (Liu *et al.*, 2012; Guo *et al.*, 2013). The monitoring site is surrounded by farms and located on the ground. As Wuxi is located on the northern shore of Taihu Lake, the site is also the generally geographic center of the most developed and polluted YRDCGA region, especially for meteorological conditions. Thus, the observations at this site could help further understand the atmospheric pollution condition in the YRDCGA and the influences from the inland or upwind polluted areas and the Taihu Lake in a regional air quality perspective.

### *Water-Soluble Inorganic Ions*

The observation of aerosol particle was conducted by using a 9-stage Anderson-type aerosol sampler (Anderson 2000 Inc., USA). The sampler has the size ranges of < 0.43, 0.43–0.65, 0.65–1.1, 1.1–2.1, 2.1–3.3, 3.3–4.7, 4.7–5.8, 5.8–9.0 and 9.0–10.0 μm for water-soluble ionic components. The samples were collected at a flow rate of 28.3 L $min^{-1}$. The measurements obtained 17 samples, each for 24 h, excluding the invalid data.

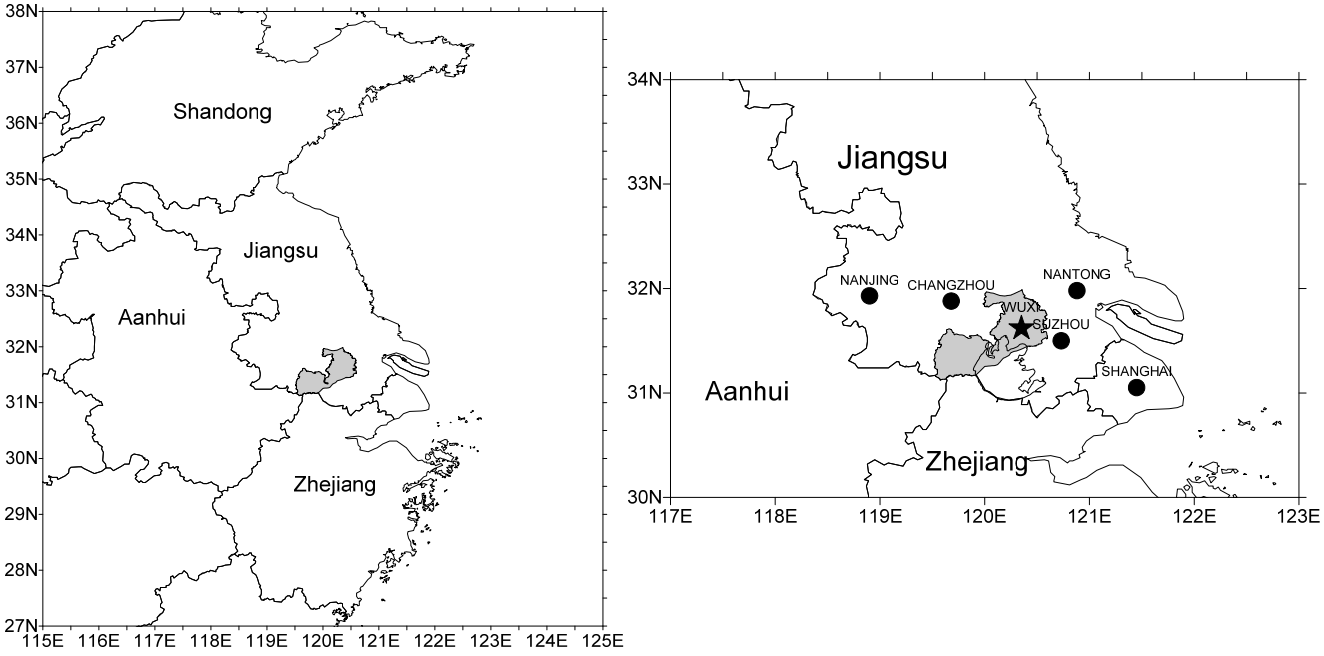


**Fig. 1.** Location of the observation site.

The sampling instrument was using the 80-mm Teflon filter (Whatman, Clifton, England) for water-soluble inorganic ionic components, the membranes were weighed by Mettler Toledo MX-5 microbalance after constant temperature (25°C) and humidity (50%) treatment for 48 h before and after sampling, and the microbalance was calibrated using standard weight. The weight difference before and after sampling is particle weight (Wang *et al.*, 2015).

The 850 Professional Ion Chromatography (IC) (Metrohm, Switzerland) was used to analyze the water-soluble inorganic ions, $NH_4^+$, $Ca^{2+}$, $Mg^{2+}$, $Na^+$, $K^+$, $Cl^-$, $NO_3^-$, $SO_4^{2-}$, $F^-$ and $NO_2^-$ were measured. Chromatography includes conductivity detector, column oven, with an 858 auto-injector and MagIC Net chromatography workstation (Metrohm, Switzerland); Metrosep C 4150/4.0 separation column and Metrosep A Supp 5150/4.0 separation column; eluent: 3.2 mmol $L^{-1}$ $Na_2CO_3$ + 1.0 mmol $L^{-1}$ $NaHCO_3$ (anions), 1.7 mmol $L^{-1}$ $HNO_3$ + 0.7 mmol $L^{-1}$ pyridine carboxylic acid (cations); column temperature: 30°C; flow rate: 1.0 mL $min^{-1}$; inject volume: 20 μL. The detection limits for $Na^+$, $NH_4^+$, $K^+$, $Mg^{2+}$, $Ca^{2+}$, $F^-$, $Cl^-$, $NO_3^-$, and $SO_4^{2-}$, were 0.001, 0.005, 0.001, 0.002,0.001, 0.04, 0.01, 0.006, 0.05 mg $L^{-1}$, respectively. Detailed information can be referred to Wang *et al.* (2015). Half of each Teflon filter was cut and placed into a 15-mL PET vial; the vial was then ultrasonically extracted for 1 h and mechanically oscillated for 1 h with 10 mL deionized water (18.2 MU). PTFE filters and filter chips were used to remove the insoluble particles before samples analyzed by IC.

### *Meteorological and Pollutant Data*

In this study, the meteorological parameters, including pressure, relative humidity (RH), precipitation, vapor pressure, dew point temperature (Td), temperature (T), visibility, wind direction (WD), wind speed (WS) and the gaseous species, including CO (48i), $NO_2$ (42i), $O_3$ (49i), and $SO_2$ (43i), and the particulate matters, including $PM_{10}$ and $PM_{2.5}$ during the sampling times, were obtained hourly from the Wuxi meteorological observational station (MOS) worked synchronously on the observation site.

## RESULTS AND DISCUSSION

### *Meiyu Period and Related Meteorological Conditions*

The Meiyu period in the middle and lower reaches of Yangtze River area mostly began in June. In 2014, the Meiyu started on June 15 at Wuxi. From Fig. 2, we can see many differences in the meteorological features or weather conditions before and during the Meiyu period. Before Meiyu, the surface vapor pressure, dew point temperature, RH (relative humidity), and the temperatures have a significant diurnal variation. The ground vapor pressure was mainly between 16 and 23 hPa, the dew point temperature fluctuated between 15 and 20°C, the RH was between 40 and 80%, and the temperature fluctuation was between 24 and 32°C. But during the Meiyu, there was more rain in Wuxi, with the ground vapor pressure increased to 24 and 28 hPa, dew point temperature mostly maintained between 20–23°C, RH remained above 75%, there was a smaller diurnal temperature variation between 24 and 28°C. But the wind speed had no change before and during the Meiyu, the wind direction maintained eastern.

### *$PM_{2.5}$, $PM_{10}$, and Related Gasses*

From Table 1, we can see that during this observation the average values of $PM_{2.5}$, $PM_{10}$, $SO_2$, $NO_2$, $O_3$, and CO were 58.5, 79.5, 21.4, 41.2, 72.9 and 772.0 μg $m^{-3}$, respectively. During Meiyu period, the mass concentrations of $PM_{10}$ and $PM_{2.5}$ were 67.2 and 50.0 μg $m^{-3}$ respectively, had a 32.5% and 34.5% decrease than before Meiyu (102.6 and 74.1 μg $m^{-3}$ respectively). The $O_3$ also have a greater decrease from 108.1 to 54.2 μg $m^{-3}$. $SO_2$ and $NO_2$ also had 59.2% and 30% drop during this period. CO changed weakly, just had 5% decreases.

As seen from Fig. 2, the $PM_{2.5}$ concentrations during observation are all under 200 μg $m^{-3}$, with a maximum of 195 μg $m^{-3}$ appears before Meiyu. The particulate matter concentrations showed an increasing trend before Meiyu, which from 40 and 60 μg $m^{-3}$ at 20:00 on June 9 increases to 195 and 277 μg $m^{-3}$ at 08:00 on June 14. Particulate matter concentrations had a significant decline during Meiyu period, the $PM_{2.5}$ and $PM_{10}$ maintained at 15–120 and 20–150 μg $m^{-3}$, respectively. During this observation, the CO, $O_3$, $SO_2$ and $NO_2$ had similar variations, and these pollution gasses changed similarly with the particulate matters.

The $O_3$ had a significant diurnal variation before Meiyu, with higher levels during the daytime, and the maximum was 327 μg $m^{-3}$. However, during the period of Meiyu $O_3$ concentration had an unapparent variation, which was related to the continuous rainy weather, and less sunshine.

### *Concentrations of Water-Soluble Inorganic Ions in Particles*

In this study, we defined the particles that Dp < 2.1 μg as the FPM (fine particle matter), and Dp > 2.1 μg as the CPM (coarse particle matter). The FPM, especially for $PM_{1.1}$, is dominant in particle matters. The FPM percentage has greater changes during this observation, especially for the $PM_{1.1}$, the $PM_{1.1}$ percentage increased from 57.8% on June 10 to 69.7% on June 15, but the CPM just have a little variation (Fig. 3(a)), changed between 20% and 30%.

From Fig. 3(b) we can see that $PM_{1.1}$ had a significant increase before Meiyu, which from 35.0 μg $m^{-3}$ to 72.4 μg $m^{-3}$ and dropped to 17.5 μg $m^{-3}$ during Meiyu. The CPM just had the peak value of 25.6 μg $m^{-3}$ before Meiyu and declined to 10.2 μg $m^{-3}$ during Meiyu. The $PM_{1.1\text{-}2.1}$ had no significant changes in characteristics before or during Meiyu. It could also be seen that before Meiyu, the $PM_{1.1}$ have increased to $PM_{1.1\text{-}2.1}$, and then to CPM. This may be because the fine aerosol particles $PM_{1.1\text{-}2.1}$ would stay a longer time in the atmosphere, and coagulation growth and chemical reaction would result in the $PM_{1.1\text{-}2.1}$ particle aging intensifying (Tröstl *et al.*, 2016).

### *Spectral Distribution of Water-Soluble Ions in Particles*

Figs. 4 and 5 show the spectral distribution of water-soluble inorganic ions. The atmospheric pollution started to develop before Meiyu (from June 10 to 15). The pollution

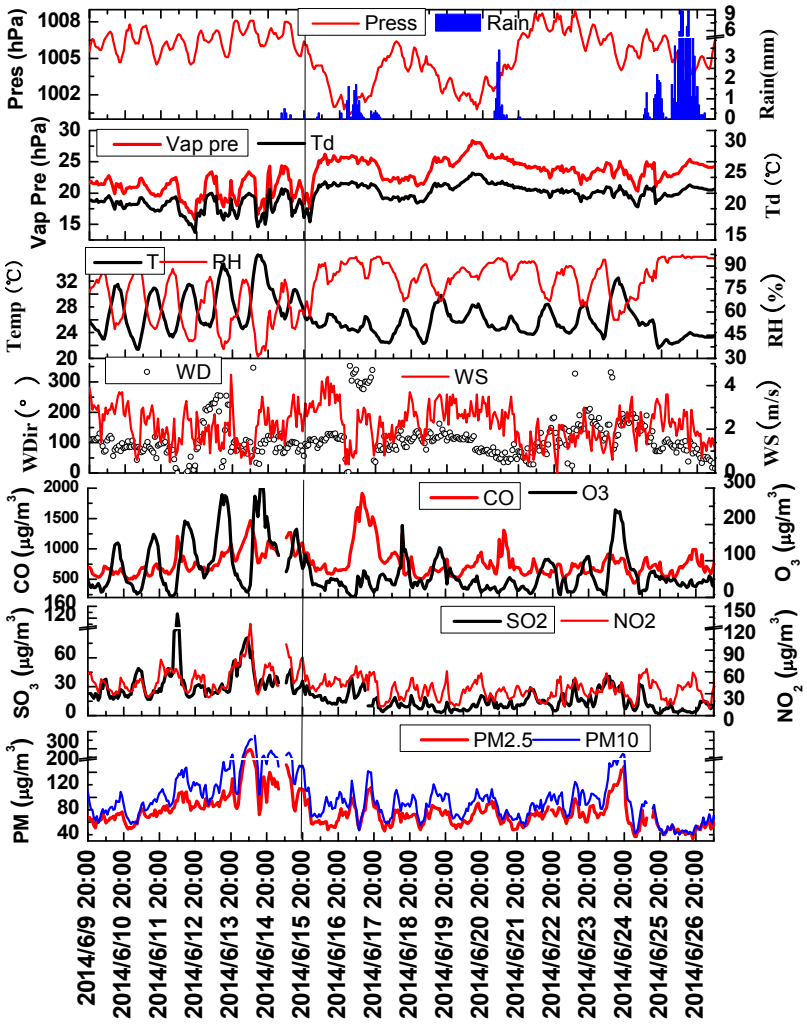


**Fig. 2.** Meteorological features and Dynamics of pollution particles and gases concentrations before and during the Meiyu period.

**Table 1.** Data of particles and the main gas before and during the Meiyu period.

| | | Max | Min | Median | Mean | S.D | before | during |
|---|---|---|---|---|---|---|---|---|
| $SO_2$ | μg $m^{-3}$ | 135.0 | 2.0 | 18.5 | 21.4 | 16.1 | 34.8 | 14.2 |
| $NO_2$ | μg $m^{-3}$ | 126.0 | 12.0 | 39.0 | 41.2 | 16.9 | 51.2 | 35.8 |
| CO | μg $m^{-3}$ | 1916.0 | 435.0 | 699.0 | 772.0 | 240.6 | 798.0 | 758.0 |
| $O_3$ | μg $m^{-3}$ | 327.0 | 2.0 | 49.0 | 72.9 | 63.4 | 108.1 | 54.2 |
| $PM_{10}$ | μg $m^{-3}$ | 277.0 | 20.0 | 73.0 | 79.5 | 39.4 | 102.6 | 67.2 |
| $PM_{2.5}$ | μg $m^{-3}$ | 195.0 | 13.0 | 53.0 | 58.5 | 27.7 | 74.1 | 50.0 |

accumulated resulted in the mass concentrations and water-soluble inorganic ions were at the highest level during this time. And then the pollution diffused and the aerosol mass concentrations decreased during Meiyu (from 16 to 26), so the mass concentrations and water-soluble inorganic ions were relatively low during this time.

Fig. 4 shows that the ions, anions, and cations all had bimodal distribution before Meiyu, and the peak positions were all at 0.43–1.1 μm (the fine mode) and 9–10 μm (the coarse mode). During the Meiyu period, they had trimodal distribution, and the peak positions were not fixed, especially for the cations. The fine particles (0.5 μm) increased remarkable before Meiyu, and the larger particles (little than 1 μm) increased shortly after it. The fine mode peaks were increased from 3.78 (10.81) to 8.80 (24.88) μg $m^{-3}$ for cations (anions) before Meiyu. However, during Meiyu period, the fine mode peaks were kept at about 4.5 (14) μg $m^{-3}$ for cations (anions).

Fig. 5 shows that the pollution effect on ions in fine particles was greater than that on ions in coarse particles, especially on $Cl^-$, $F^-$, and $K^+$. The peak values of $K^+$ and $F^-$ are both appeared at 0.2 μm, and $Cl^-$ appeared at 0.43–1.1 μm. $Cl^-$ and $K^+$ produced by the biomass burning mainly distributed in fine particles below 1 μm, which confirmed

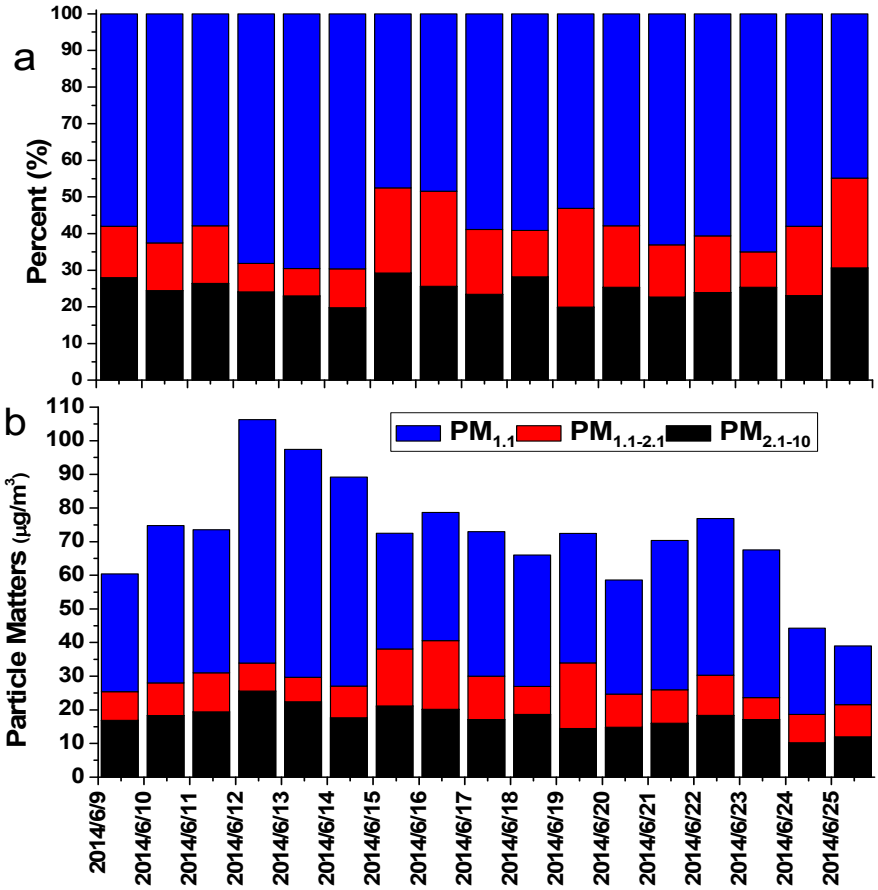


**Fig. 3.** Dynamics of particle matter (a) percentageand (b) concentrations at Wuxi from 10 to 26 June 2014.

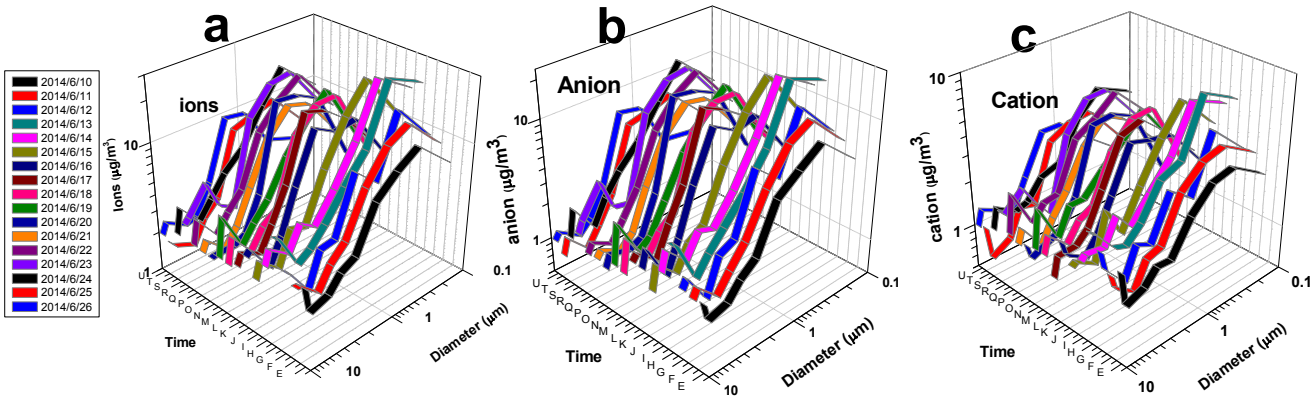


**Fig. 4.** Spectral distribution of water soluble inorganic ionic, anion, and cation (The time coordinates are from E (June 10, 2014) to U (June 26, 2014), The diameter coordinate are from 0.1 μm to 10 μm, The ions coordinate are the concentrations for ionic, anion, and cation respectively).

the general conclusion that $Cl^-$ and $K^+$ were mainly from crop-straw burning (Zhang *et al.*, 2013; Yan *et al.*, 2015; Sun *et al.*, 2016).

The size spectrum of $Ca^{2+}$, $Mg^{2+}$ and $Na^+$ changed greatly, they were in multimodal distribution, and its peak value was unfixed, which may be associated with the observation site geographical location. The mass concentrations in coarse particles are similar with fine particles. This is because the $Ca^{2+}$ mainly comes from the construction dust, $Mg^{2+}$, and $Na^+$ mainly from soil dust and sea, thus these three ions mainly appeared in the coarse particles, it also suggests that the $Ca^{2+}$ and $Mg^{2+}$ distributions may be impacted by the location area (Zhang *et al.*, 2013; Yan *et al.*, 2015; Sun *et al.*, 2016).

The $SO_4^{2-}$, $NO_3^-$ and $NH_4^+$ spectral size distributions were almost the same on normal and pollution days, they all in bimodal distribution or trimodal distribution before Meiyu, the mass concentration of fine particles were all

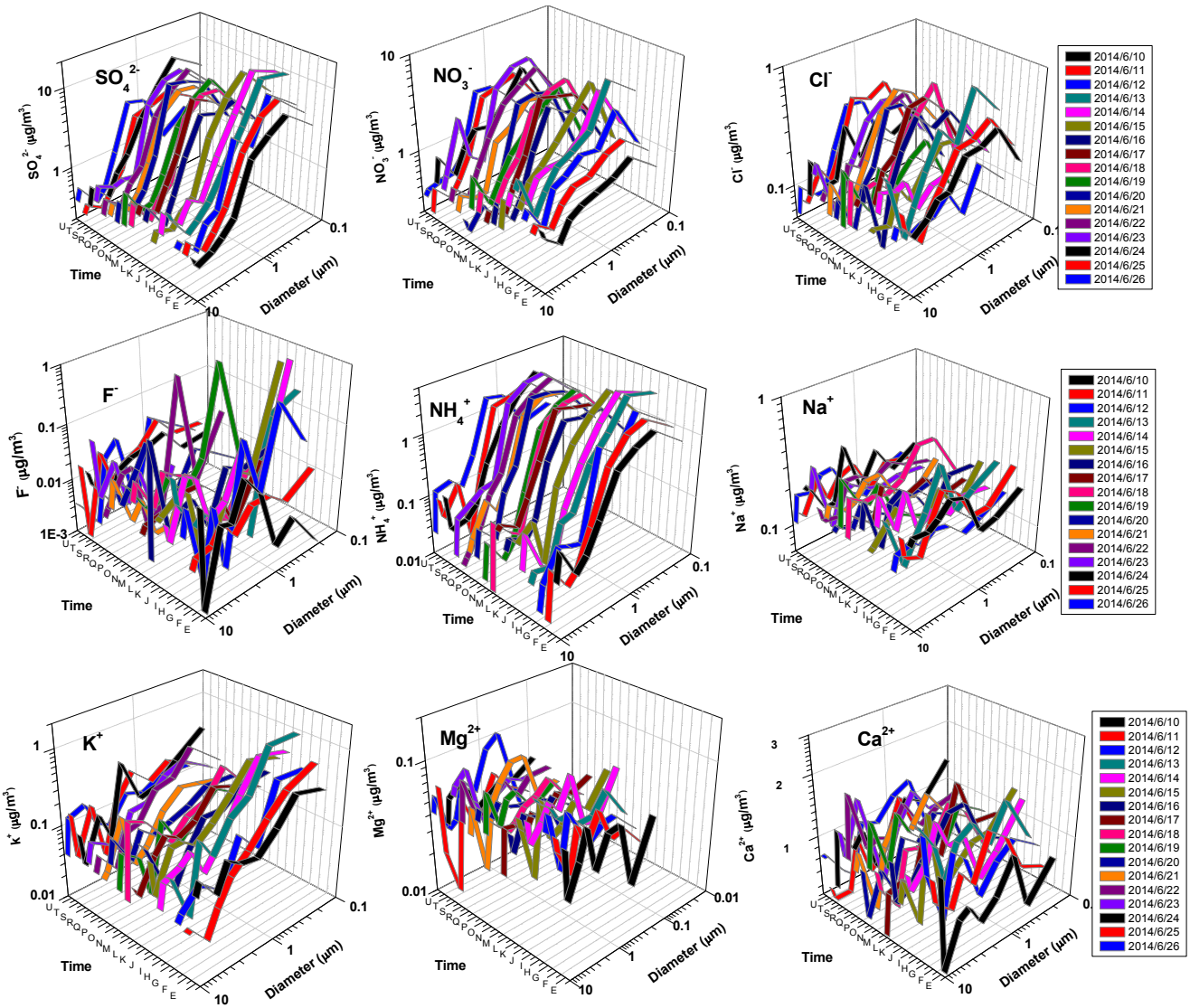


**Fig. 5.** Spectral distribution of water-soluble ionic (The time coordinates are from E (June 10, 2014) to U (June 26, 2014), The diameter coordinate are from 0.1 μm to 10 μm, The ions coordinate are the concentrations for ionics respectively).

greater than that in coarse particles. There was a common trend for these three ions, that the first peak kept 0.43–0.65 μm, with the value were about 13, 6.0, 5.0 μg $m^{-3}$ for $SO_4^{2-}$, $NO_3^-$, and $NH_4^+$ before Meiyu, but they decreased to 8.0, 3.0, 2.0 μg $m^{-3}$ for $SO_4^{2-}$, $NO_3^-$, and $NH_4^+$ during Meiyu. We can speculate that the sulfate, nitrate, and amine salt cumulated in the atmosphere by gas-particle transition during the continuous pollution weather before Meiyu, and then the pollution gas concentrations decreased during Meiyu period led the weaken of gas-particle conversion, and the $SO_4^{2-}$, $NO_3^-$ and $NH_4^+$ decrease (Wang *et al.*, 2012a; Sun *et al.*, 2016;).

### *Ionic Species*

*The Second Inorganic Ions and the Source of $SO_4^{2-}$ and $NO_3^-$*

There were less $SO_4^{2-}$, $NO_3^-$, $NH_4^+$ (SNA) in $PM_{2.1\text{-}10}$, and most of them are from the pollution gas secondary conversion. The relationships between the particle matters ($PM_{1.1}$, $PM_{1.1\text{-}2.1}$ and $PM_{2.1\text{-}10}$) and the second inorganic ions ($SO_4^{2-}$, $NO_3^-$, and $NH_4^+$) are presented in Table 2. SNA are the main components of the $PM_{1.1}$ and $PM_{1.1\text{-}2.1}$, the SNA concentrations are significantly correlated with the mass concentrations of the $PM_{1.1}$ and $PM_{1.1\text{-}2.1}$. From Table 2, we can see that the SNA in $PM_{1.1}$ and $PM_{1.1\text{-}2.1}$ increased quickly before Meiyu. The SNA in $PM_{1.1}$ rose from 28.44 μg $m^{-3}$ in June 10 to 61.13 μg $m^{-3}$ in June 13, and the SNA in $PM_{1.1\text{-}2.1}$ rose from 6.35 μg $m^{-3}$ in June 10 to 9.69 μg $m^{-3}$ in June 12 (Table 2). The $SO_4^{2-}$ proportions of SNA in $PM_{1.1}$ and $PM_{1.1\text{-}2.1}$ are exceeding 60% and 50% before Meiyu, respectively. During Meiyu, the SNA in $PM_{1.1\text{-}2.1}$ has a slight decline and maintain at 35 μg $m^{-3}$. And the $SO_4^{2-}$ proportions of SNA in $PM_{1.1}$ are all below 60%. However, the SNA in $PM_{1.1\text{-}2.1}$ has a remarkable increase during Meiyu, with the maximum value was 18.04 μg $m^{-3}$ on June 17. And the $SO_4^{2-}$ proportions of SNA in $PM_{1.1\text{-}2.1}$ are all below 50%.

In order to indicate the relative importance of stationary

**Table 2.** Relationships between $SO_4^{2-}$, $NO_3^-$, and $NH_4^+$ in different sizes of particles.

| | SNA | $SO_4^{2-}$/SNA | $NO_3^-$/$SO_4^{2-}$ | SNA | $SO_4^{2-}$/SNA | $NO_3^-$/$SO_4^{2-}$ | SNA | $SO_4^{2-}$/SNA | $NO_3^-$/$SO_4^{2-}$ | SNA | $SO_4^{2-}$/SNA | $NO_3^-$/$SO_4^{2-}$ |
|---|---|---|---|---|---|---|---|---|---|---|---|---|
| | $PM_{10}$ | | | $PM_{2.1\text{-}10}$ | | | $PM_{1.1\text{-}2.1}$ | | | $PM_{1.1}$ | | |
| 2014/6/10 | 42.79 | 0.63 | 0.31 | 8.00 | 0.43 | 1.09 | 6.35 | 0.66 | 0.25 | 28.44 | 0.68 | 0.18 |
| 2014/6/11 | 54.71 | 0.64 | 0.31 | 8.81 | 0.45 | 1.14 | 6.89 | 0.64 | 0.30 | 39.00 | 0.68 | 0.19 |
| 2014/6/12 | 54.62 | 0.58 | 0.45 | 9.29 | 0.39 | 1.49 | 9.69 | 0.59 | 0.35 | 35.65 | 0.62 | 0.31 |
| 2014/6/13 | 79.14 | 0.55 | 0.53 | 12.68 | 0.41 | 1.35 | 5.32 | 0.45 | 0.83 | 61.13 | 0.59 | 0.39 |
| 2014/6/14 | 75.16 | 0.62 | 0.35 | 11.28 | 0.43 | 1.21 | 5.06 | 0.55 | 0.51 | 58.82 | 0.66 | 0.23 |
| 2014/6/15 | 69.42 | 0.59 | 0.41 | 8.79 | 0.39 | 1.34 | 7.56 | 0.55 | 0.48 | 53.08 | 0.63 | 0.30 |
| 2014/6/16 | 53.04 | 0.54 | 0.52 | 11.55 | 0.54 | 0.66 | 13.96 | 0.51 | 0.60 | 27.53 | 0.56 | 0.44 |
| 2014/6/17 | 60.09 | 0.52 | 0.56 | 11.55 | 0.56 | 0.58 | 18.04 | 0.54 | 0.48 | 30.5 | 0.50 | 0.59 |
| 2014/6/18 | 54.45 | 0.50 | 0.65 | 8.28 | 0.44 | 1.08 | 10.69 | 0.49 | 0.63 | 35.48 | 0.51 | 0.57 |
| 2014/6/19 | 47.66 | 0.56 | 0.48 | 8.13 | 0.48 | 1.02 | 6.67 | 0.55 | 0.47 | 32.87 | 0.58 | 0.37 |
| 2014/6/20 | 57.23 | 0.60 | 0.35 | 6.99 | 0.61 | 0.47 | 17.43 | 0.62 | 0.30 | 32.81 | 0.59 | 0.36 |
| 2014/6/21 | 41.8 | 0.56 | 0.47 | 6.98 | 0.48 | 0.93 | 7.68 | 0.57 | 0.38 | 27.14 | 0.57 | 0.4 |
| 2014/6/22 | 51.82 | 0.52 | 0.59 | 7.12 | 0.45 | 1.09 | 7.68 | 0.47 | 0.73 | 37.02 | 0.54 | 0.49 |
| 2014/6/23 | 59.29 | 0.47 | 0.75 | 9.23 | 0.37 | 1.57 | 9.99 | 0.45 | 0.77 | 40.07 | 0.50 | 0.61 |
| 2014/6/24 | 50.12 | 0.59 | 0.44 | 8.50 | 0.41 | 1.29 | 4.84 | 0.58 | 0.45 | 36.78 | 0.63 | 0.31 |
| 2014/6/25 | 31.03 | 0.43 | 0.85 | 4.40 | 0.44 | 1.02 | 6.44 | 0.41 | 0.92 | 20.19 | 0.44 | 0.79 |
| 2014/6/26 | 25.39 | 0.45 | 0.80 | 5.24 | 0.48 | 0.82 | 7.78 | 0.46 | 0.71 | 12.37 | 0.44 | 0.86 |

vs. mobile sources of nitrogen and sulfur in the atmosphere, the $[NO_3^-]/[SO_4^{2-}]$ mass ratio has been analyzed (Arimoto *et al.*, 1996; Yao *et al.*, 2002). In China, diesel fuel and gasoline contain 0.2% and 0.12% sulfur (by weight), respectively (Kato, 1996). And the estimated $SO_2$ to $NO_x$ ratios from the emission of diesel fuel and gasoline burning are 1:8 and 1:13, respectively. The lower $[NO_3^-]/[SO_4^{2-}]$ ratios (e.g., 0.1–0.7, according to Yao *et al.* (2002)) have usually been found in China since the wide use of sulfur-containing coal. The average mass ratios of $[NO_3^-]/[SO_4^{2-}]$ are 0.6 during haze and 0.27 during non-haze in Nanjing, China (Zhou *et al.*, 2015).

From Table 2, the $[NO_3^-]/[SO_4^{2-}]$ ratios of $PM_{1.1}$ and $PM_{1.1\text{-}2.1}$ varied between 0.18 and 0.39 (for $PM_{1.1}$) and 0.25–0.83 (for $PM_{1.1\text{-}2.1}$) with an annual average of 0.26 and 0.45 in Wuxi during pre-Meiyu. However, during the Meiyu period, the ratio varied between 0.30 and 0.86 for $PM_{1.1}$ and 0.30–0.92 for $PM_{1.1\text{-}2.1}$. The low-mass ratios suggest that during this observation period the emissions of the stationary source were more important than that of vehicle source in the source areas. In most time of this observation period, the vehicle emissions were larger in $PM_{1.1\text{-}2.1}$ than in $PM_{1.1}$.

Compared the pre-Meiyu and during Meiyu, the vehicle emissions were larger during Meiyu than pre-Meiyu. It is suggested that vehicle emissions are more important during Meiyu than pre-Meiyu.

*The Formation Processes of $SO_4^{2-}$ and $NO_3^-$*

To indicate the aerosol secondary transformation processes from $SO_2$ or $NO_x$, the sulfur oxidation ratio (SOR [SOR = $SO_4^{2-}/(SO_4^{2-} + SO_2)$]) and nitrogen oxidation ratio (NOR [NOR = $NO_3^-/(NO_3^- + NO_x)$]) were defined in this study (Cao *et al.*, 2012). Fig. 6(a) shows the SOR and NOR acquired for aerosols in Wuxi. The average SOR values were 0.60, 0.52, and 0.65, during the whole observation period, pre-Meiyu, and during-Meiyu, respectively. The corresponding values for NOR were 0.29, 0.25, and 0.32, respectively. SOR shows the sulfur oxidation degree in terms of the ratio of the sulfur in sulfate to the total sulfur. Likewise, the NOR shows the nitrogen oxidation degree in terms of the ratio of the nitrogen in nitrate to the total nitrogen. Higher SOR and NOR suggest that the gaseous species oxidation would occur and more secondary aerosols would reside in the atmosphere.

Earlier researchers have shown that the SOR value is lower than 0.10 in the primary pollutant (Pierson *et al.*, 1979; Truex *et al.*, 1980). Ohta and Okita (1990) reported that when the ratio value was larger than 0.10, $SO_2$ photochemical oxidation would take place in the atmosphere. The SOR and NOR in Wuxi aerosols were both higher than 0.10 in June. From Fig. 6(a) we can see that the SOR varied between 0.41 and 0.59 and the NOR varied between 0.21 and 0.37 during pre-Meiyu. However, during the Meiyu period, the SOR varied between 0.52 and 0.79 and the NOR varied between 0.22 and 0.41. The result clearly suggested that the $SO_4^{2-}$ secondary formation from $SO_2$ occurred easier during Meiyu than pre-Meiyu. The NOR distribution in the observation period was similar with that of SOR. NOR was generally lower than SOR, which is similar with Beijing (Wang *et al.*, 2005). The lower NOR in Wuxi aerosols showed that the $NO_3^-$ secondary formation from $NO_x$ weakly occurred in Wuxi compared to that of $SO_4^{2-}$.

From Figs. 2, 5, and 6(a) we can see that, during June 18 and 21 the vapor pressure and the relative humidity (RH) have an obvious relation with the SOR. Under the condition of high humidity and high vapor pressure, it is easier for $SO_4^{2-}$ secondary formation from $SO_2$. The NOR increased during June 16, 22, and 23, it was the time that the wind speed were lower than 2 m $s^{-1}$, and under the condition of high humidity and high vapor pressure.

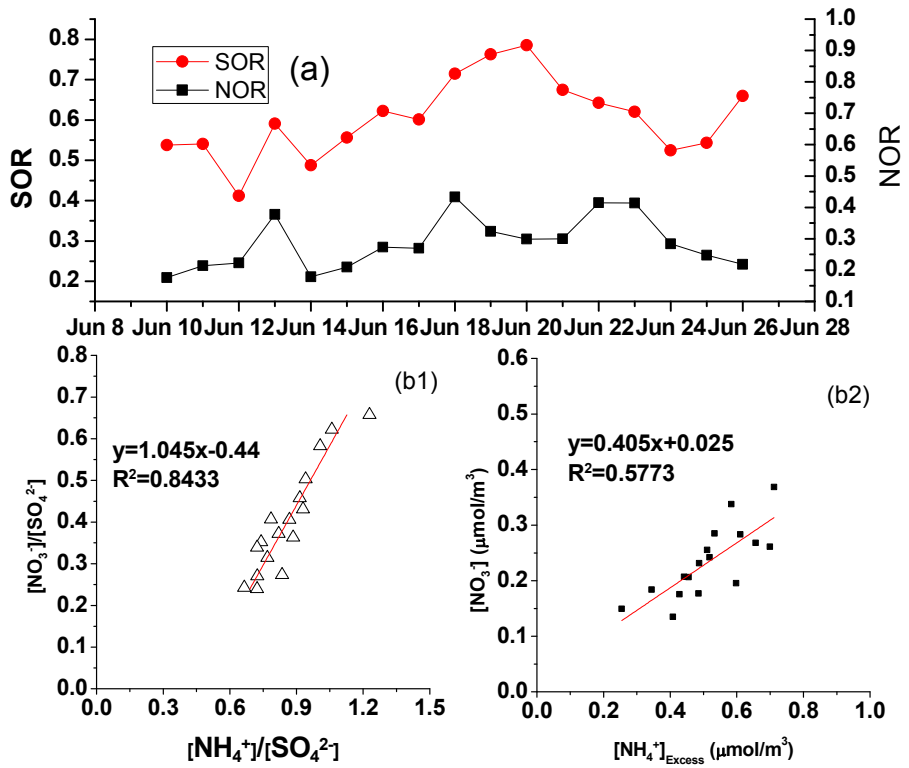


**Fig. 6.** Temporal variation of (a) SOR [SOR = $SO_4^{2-}/(SO_4^{2-} + SO_2)$] and NOR [NOR = $NO_3^-/(NO_3^- + NO_x)$], (b1) the data plots of $[NO_3^-]/[SO_4^{2-}]$ and $[NH_4^+]/[SO_4^{2-}]$, and (b2) $NO_3^-$ concentration as a function of $[NH_4^+]_{Excess}$.

Fig. 6(b1) presented the relationship data plots between $[NO_3^-]/[SO_4^{2-}]$ and $[NH_4^+]/[SO_4^{2-}]$. Significant linear correlations display the prevailing of gas-phase homogeneous reaction between $HNO_3$ and $NH_3$ (Pathak *et al.*, 2009), and the regression curve between $[NO_3^-]/[SO_4^{2-}]$ and $[NH_4^+]/[SO_4^{2-}]$ is ($R^2 = 0.8433$, n = 17):

$$\frac{[NO_3^-]}{[SO_4^{2-}]} = 1.045\frac{[NH_4^+]}{[SO_4^{2-}]} - 0.44\frac{[NO_3^-]}{[SO_4^{2-}]} = 1.045\frac{[NH_4^+]}{[SO_4^{2-}]} - 0.44 \quad (1)$$

The regression curve slope (1.045) is approximately equal to 1, which is fit in with the $NH_4^+$ and $NO_3^-$ mole ratio in $NH_4NO_3$ that indicates almost all $NO_3^-$ has been neutralized by $NH_4^+$. On this occasion, $NH_4^+$ is not enough to react with a large proportion of $SO_4^{2-}$ or $HSO_4^-$ to form $(NH_4)_2SO_4$ or $NH_4HSO_4$. The $NH_4^+$ is valuable for the $NH_4NO_3$ formation (He *et al.*, 2012), which can be derived from Eq. (2) (0.92 is the regression curve intercept with the axis of $[NH_4^+]/[SO_4^{2-}]$):

$$[NH_4^+]_{Excess} = \left(\frac{[NH_4^+]}{[SO_4^{2-}]} - 0.92\right) \times [SO_4^{2-}] \quad (2)$$

Fig. 6(b2) showed the significant linear relationship ($R^2 = 0.5773$) between $[NH_4^+]_{Excess}$ and $NO_3^-$. It confirms the importance of gas reaction for acidic samples. Meanwhile, the regression curve slope of 0.405 suggests that not all $NO_3^-$ can be neutralized by $NH_4^+$, thus $NH_4^+$ is not enough to react with a large proportion of $SO_4^{2-}$ or $HSO_4^-$ to form $(NH_4)_2SO_4$ or $NH_4HSO_4$; this will be discussed in Section 3.5.3.

*Quantitative Analyses of Cations and Anions in Particles*

The acidity of $PM_{2.5}$ is usually evaluated by AE (anion equivalence) vs. CE (cation equivalence), which is calculated by transforming the anion and cation concentrations (μg $m^{-3}$) into micro-equivalents (μmol $m^{-3}$) by the Eqs. (3) and (4) (Meng *et al.*, 2016):

$$AE = \frac{SO_4^{2-}}{48} + \frac{NO_3^-}{62} + \frac{NO_2^-}{46} + \frac{Cl^-}{35.5} \quad (3)$$

$$CE = \frac{NH_4^+}{18} + \frac{Na^+}{23} + \frac{Mg^{2+}}{12} + \frac{Ca^{2+}}{20} + \frac{K^+}{39} \quad (4)$$

Fig. 7(a) illustrates the relationship data plots of AE vs. CE from June 10 to June 26, 2014. Ten ions measured in this period are the major compositions of $PM_{2.5}$ ionic constituents in Wuxi, which can be sustained by the existence of strong correlations (~1.0) between CE and AE during this observation period. The samples collected in pre-Meiyu and during Meiyu are all plotted below the 1:1 (CE:AE) curve, which suggests that the volatilization of ammonium and nitrate as well as unmeasured hydrogen ions may

cause the loss of cations, resulting in an insufficient number of cations for neutralizing the anions and therefore acidic properties for the aerosol.

Figs. 7(b)–7(j) depicts the data plots of $NH_4^+$ vs. $SO_4^{2-}$, $[SO_4^{2-} + NO_3^-]$, $[SO_4^{2-} + NO_3^- + NO_2^- + Cl^-]$, $Ca^{2+}$ vs. $SO_4^{2-}$, $[SO_4^{2-} + NO_3^-]$, $[SO_4^{2-} + NO_3^- + NO_2^- + Cl^-]$, and $[NH_4^+ + Ca^{2+}]$ vs. $SO_4^{2-}$, $[SO_4^{2-} + NO_3^-]$, $[SO_4^{2-} + NO_3^- + NO_2^- + Cl^-]$ during June 10 and 26, 2014, respectively, to further inquire into the relationship between $NH_4^+$, $Ca^{2+}$ and major other acidic ions, i.e., $SO_4^{2-} + NO_3^-$, $NO_2^-$ and $Cl^-$. Suggest that electron equivalent concentrations are used over all this section.

From the Figs. 7(b)–7(d) ($NH_4^+$ vs. $SO_4^{2-}$, $[SO_4^{2-} + NO_3^-]$, $[SO_4^{2-} + NO_3^- + NO_2^- + Cl^-]$), data plots are positioned below the 1:1 curve indicates that $NH_4^+$ is not sufficient to neutralize the $SO_4^{2-}$, $[SO_4^{2-} + NO_3^-]$, and $[SO_4^{2-} + NO_3^- + NO_2^- + Cl^-]$ in most samples. There are just two samples that $NH_4^+$ is equally sufficient to neutralize $SO_4^{2-}$, and thus in these two samples $SO_4^{2-}$ presence in the case of $(NH_4)_2SO_4$. Commonly, regardless of the source models or receptor models, we always presume that $SO_4^{2-}$ has precedence over $NO_3^-$ to associate with $NH_4^+$, while actually $NH_4NO_3$ is also slowly produced in the atmosphere (Meng *et al.*, 2016). As $NH_4^+$ has insufficient conditions, $NH_4^+$ is not adequate to neutralize $SO_4^{2-}$, $NO_3^-$, $NO_2^-$, and $Cl^-$ in the meantime, therefore the exists of $NO_3^-$ is in the case of $NH_4NO_3$ and $HNO_3$, $Cl^-$ is in the case of KCl since the good correlation between $Cl^-$ and $K^+$ ($r = 0.8$, $n = 91$).

From Figs. 7(e)–7(g) ($Ca^{2+}$ vs. $SO_4^{2-}$, $[SO_4^{2-} + NO_3^-]$, $[SO_4^{2-} + NO_3^- + NO_2^- + Cl^-]$), the $Ca^{2+}$ has the similar situation with $NH_4^+$. There are just two samples that $Ca^{2+}$ is equally sufficient to neutralize $SO_4^{2-}$, and thus in these two samples $SO_4^{2-}$ is present in the form of $CaSO_4$ (Fig. 7(e)). Data plots are mostly positioned below the 1:1 line, indicating that $Ca^{2+}$ is also not sufficient to neutralize $SO_4^{2-}$, $[SO_4^{2-} + NO_3^-]$, and $[SO_4^{2-} + NO_3^- + NO_2^- + Cl^-]$ in most samples.

What about $[NH_4^+ + Ca^{2+}]$ vs. $SO_4^{2-}$, $[SO_4^{2-} + NO_3^-]$, $[SO_4^{2-} + NO_3^- + NO_2^- + Cl^-]$? According to the Fig. 7(h), data plots are positioned above the 1:1 line indicating that $[NH_4^+ + Ca^{2+}]$ is equal to neutralize $SO_4^{2-}$, and therefore in all samples $SO_4^{2-}$ exists in the case of $(NH_4)_2SO_4$ or $CaSO_4$. And from Fig. 7(i), data plots are also positioned above the 1:1 line indicating that $[NH_4^+ + Ca^{2+}]$ is fairly sufficient to neutralize $[SO_4^{2-} + NO_3^-]$, and therefore in all samples $SO_4^{2-}$ and $NO_3^-$ exists in the case of $(NH_4)_2SO_4$, $CaSO_4$, $NH_4NO_3$ and $Ca(NO_3)_2$.

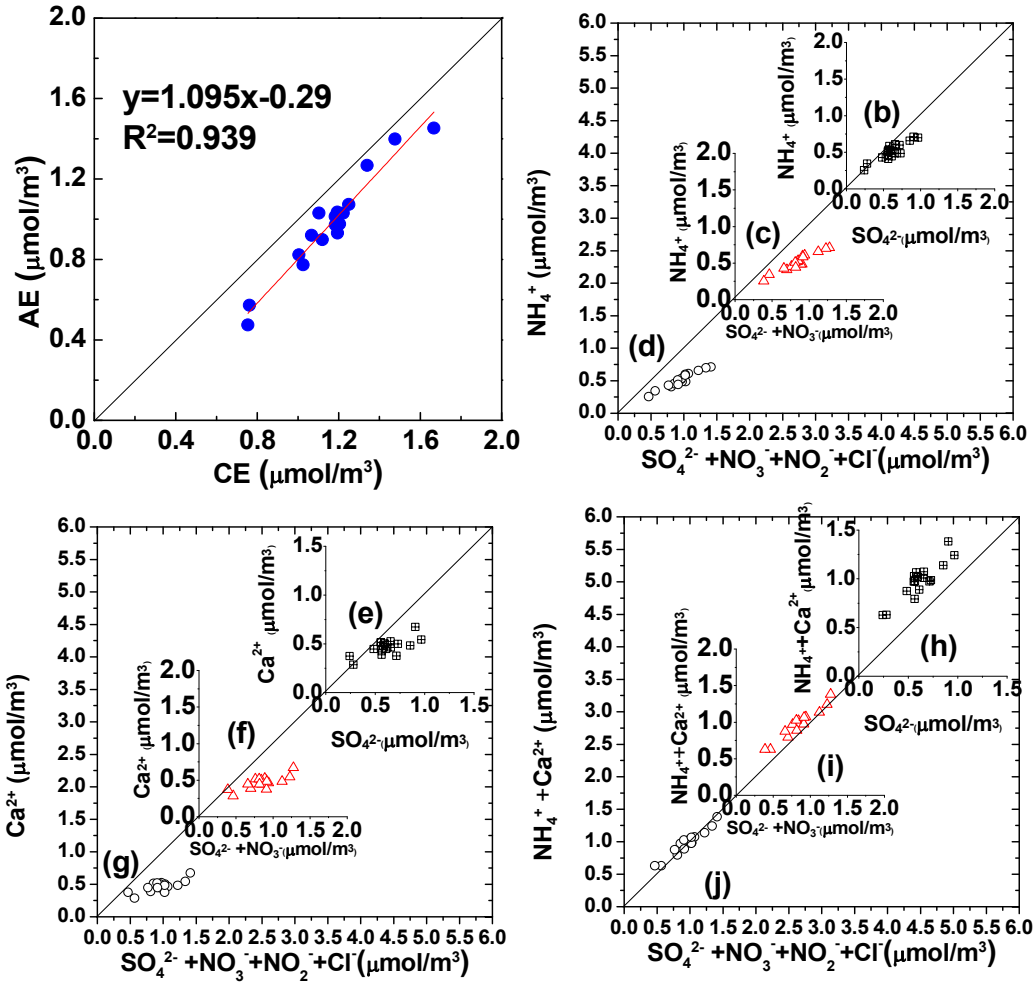


**Fig. 7.** (a) Plot of cations concentration vs. anions concentration and (b–j) the data plot of ammonium, calcium and the major acidic ions for particle matters of Wuxi in June 2014.

All the data points in Fig. 7(j) are above or near the 1:1 curve, which suggests that [$NH_4^+$ + $Ca^{2+}$] are evidently sufficient to neutralize [$SO_4^{2-}$ + $NO_3^-$ + $NO_2^-$ + $Cl^-$].

## CONCLUSION

In this study, the size distributions and water-soluble inorganic ions of aerosol were measured between June 10 and 26, 2014, which spanned the pre-Meiyu and Meiyu periods, on the north shore of Taihu Lake. A total of seventeen samples were measured, and the species variation patterns were investigated in detail.

The particulate matter concentrations showed an increasing trend before Meiyu and a significant decline during Meiyu, and the gas pollutants (CO, $O_3$, $SO_2$, and $NO_2$) similarly changed. Prior to Meiyu, the $PM_{1.1}$ increased to $PM_{1.1\text{-}2.1}$ and then to CPM due to coagulation growth and chemical reactions. Also at this time, a remarkable increase was displayed by the $NO_3^-$ and $NH_4^+$ in the $PM_{1.1}$ and $PM_{1.1\text{-}2.1}$ and by the $Ca^{2+}$ in the $PM_{2.1\text{-}10}$.

The ions, anions, and cations exhibited bimodal distributions before Meiyu, showing peak positions of 0.43–1.1 μg and 9–10 μg. During Meiyu, however, they exhibited trimodal distributions, and the peak positions remained unfixed, especially for the cations. The size spectra of $Ca^{2+}$, $Mg^{2+}$, and $Na^+$ changed greatly; they exhibited multimodal distributions, and their peak positions were unfixed.

All of the spectral size distributions of $SO_4^{2-}$, $NO_3^-$, and $NH_4^+$ were bimodal or trimodal before Meiyu, and the mass concentrations were greater in the fine particles than the coarse ones. The sulfate, nitrate, and amine salt accumulated in the atmosphere by gas-particle conversion during the continuous weather pollution prior to Meiyu, but the gas-pollutant concentrations decreased during Meiyu, which led to weakened gas-particle conversion and decreased $SO_4^{2-}$, $NO_3^-$, and $NH_4^+$.

Less $SO_4^{2-}$, $NO_3^-$, and $NH_4^+$ exists in $PM_{2.1\text{-}10}$, and most it is from the secondary conversion of gas pollutants. SNA is the main component of the $PM_{1.1}$ and $PM_{1.1\text{-}2.1}$, and its concentration variations are significantly correlated with the mass concentrations of the $PM_{1.1}$ and $PM_{1.1\text{-}2.1}$. During this observation period, emissions from the stationary source were more important than those from vehicle sources in the source areas. During most of the observation period, vehicle emissions were larger in $PM_{1.1\text{-}2.1}$ than in $PM_{1.1}$; they were also more important during Meiyu than pre-Meiyu. The secondary formation of $SO_4^{2-}$ from $SO_2$ also occurred more readily during Meiyu than before Meiyu. The NOR was lower than the SOR. The secondary formation of $NO_3^-$ from $NO_x$ infrequently occurred in Wuxi compared to that of $SO_4^{2-}$ from $SO_2$.

All of the samples collected before and during Meiyu were plotted below the 1:1 (CE:AE) curve, suggesting that the volatilization of ammonium and nitrate, as well as unmeasured hydrogen ions, may cause the loss of cations, which prevents the anions from being neutralized and leads to the aerosol displaying acidic properties. In most of the samples, both the $NH_4^+$ and the $Ca^{2+}$ were insufficient for neutralizing the $SO_4^{2-}$, [$SO_4^{2-}$ + $NO_3^-$], and [$SO_4^{2-}$ + $NO_3^-$ + $NO_2^-$ + $Cl^-$]. In all of the samples, the [$NH_4^+$ + $Ca^{2+}$] was fairly sufficient for neutralizing the $SO_4^{2-}$—which was therefore present as $(NH_4)_2SO_4$ or $CaSO_4$—and the [$SO_4^{2-}$ + $NO_3^-$]—which was present in the form of $(NH_4)_2SO_4$, $CaSO_4$, $NH_4NO_3$, and $Ca(NO_3)_2$. The [$NH_4^+$ + $Ca^{2+}$] was also evidently sufficient for neutralizing the [$SO_4^{2-}$ + $NO_3^-$ + $NO_2^-$ + $Cl^-$].

These results have implications for understanding the impact of biomass burning emissions on the regional air quality and climate over YRDCGA and designing appropriate mitigation strategies.

## ACKNOWLEDGEMENTS

This work was financially supported jointly by the National Key R&D Program of China (2016YFC0203303 and 2016YFC0201903), the National Natural Science Foundation of China (41575135), and the 333 Project of Jiangsu Province (BRA2016565).

## REFERENCE

Arimoto, R., Duce, R.A., Savoie, D.L., Prospero, J.M., Talbot, R., Cullen, J.D., Tomza, U., Lewis, N.F. and Ray, B.J. (1996). Relationships among aerosol constituents from Asia and the North Pacific during PEM-West A. *J. Geophys. Res.* 101: 2011–2023.

Bisht, D.S., Dumka, U.C., Kaskaoutis, D.G., Pipal, A.S., Srivastava, A.K., Soni, V.K., Attri, S.D., Sateesh, M. and Tiwari, S. (2015). Carbonaceous aerosols and pollutants over Delhi urban environment: Temporal evolution, source apportionment and radiative forcing. *Sci. Total Environ.* 521–522: 431–445.

Cao, J.J., Wang, Q.Y., Chow, J.C., Watson, J.G., Tie, X.X., Shen, Z.X., Wang, P. and An, Z.S. (2012). Impacts of aerosol compositions on visibility impairment in Xi'an, China. *Atmos. Environ.* 59: 559–566.

Cheng, M.C., You, C.F., Cao, J. and Jin, Z. (2012). Spatial and seasonal variability of water-soluble ions in $PM_{2.5}$ aerosols in 14 major cities in China. *Atmos. Environ.* 60: 182–192.

Ding, A., Wang, T. and Fu, C. (2013). Transport characteristics and origins of carbon monoxide and ozone in Hong Kong, South China. *J. Geophys. Res.* 118: 9475–9488.

Du, H., Kong, L., Cheng, T., Chen, J., Du, J., Li, L., Xia, X., Leng, C. and Huang, G. (2011). Insights into summertime haze pollution events over Shanghai based on online water-soluble ionic composition of aerosols. *Atmos. Environ.* 45: 5131–5137.

Gao, J., Peng, X., Chen, G., Xu, J., Shi, G.L., Zhang, Y.C. and Feng, Y.C. (2016). Insights into the chemical characterization and sources of $PM_{2.5}$ in Beijing at a 1-h time resolution. *Sci. Total Environ.* 542: 162–171.

Guo, Y.F., Liu, D.Y., Zhou, B., Xia, J., Wu, Y. and Hu, Y.H. (2013). Study on haze characteristics in Wuxi and its impact factors. *Meteorol. Mon.* 39: 1314–1324 (in Chinese).

He, K., Zhao, Q., Ma, Y., Duan, F., Yang, F., Shi, Z. and Chen, G. (2012). Spatial and seasonal variability of $PM_{2.5}$ acidity at two Chinese megacities: Insights into the formation of secondary inorganic aerosols. *Atmos. Chem. Phys*. 12: 1377–1395.

He, Q., Zhao, X., Lu, J., Zhou, G., Yang, H., Gao, W., Yu, W. and Cheng, T. (2015). Impacts of biomass-burning on aerosol properties of a severe haze event over Shanghai. *Particuology* 20: 52–60.

Huang, X., Liu, Z., Zhang, J., Wen, T., Ji, D. and Wang, Y. (2016). Seasonal variation and secondary formation of size-segregated aerosol water-soluble inorganic ions during pollution episodes in Beijing. *Atmos. Res.* 168: 70–79.

Huang, X.F., Yu, J.Z., He, L.Y. and Yuan, Z. (2006). Water-soluble organic carbon and oxalate in aerosols at a coastal urban site in China: Size distribution characteristics, sources, and formation mechanisms. *J. Geophys. Res.* 111: D22212.

Jiang, N., Guo, Y., Wang, Q., Kang, P., Zhang, R. and Tang, X. (2017). Chemical composition characteristics of $PM_{2.5}$ in three cities in Henan, Central China. *Aerosol Air Qual. Res.* 17: 2367–2380.

Kato, N. (1996). Supercities: Environment quality and sustainable development analysis of structure of energy consumption and dynamics of emission of atmospheric species related to the global environmental change ($SO_x$, $NO_x$, and $CO_2$) in Asia. *Atmos. Environ.* 30: 757–785.

Li, J., Song, Y., Mao, Y., Mao, Z., Wu, Y., Li, M., Huang, X., He, Q. and Hu, M. (2014). Chemical characteristics and source apportionment of $PM_{2.5}$ during the harvest season in eastern China's agricultural regions. *Atmos. Environ.* 92: 442–448.

Li, Y.C., Shu, M., Ho, S.S.H., Yu, J.Z., Yuan, Z.B., Wang, X.X., Zhao, X.Q. and Liu, Z.F. (2018). Effects of chemical composition of $PM_{2.5}$ on visibility in a semi-rural city of Sichuan Basin. *Aerosol Air Qual. Res.* 18: 957–968.

Liang, D., Ma, X., Zhang, J., Liu, Z., Wu, J., Feng, Y. and Zhang, Y. (2017). Chemical Analysis of particulate matter in the harvest period in an agricultural region of Eastern China. *Aerosol Air Qual. Res.* 17: 2381–2389.

Liu, B., Song, N., Dai, Q., Mei, R., Sui, B., Bi, X. and Feng, Y. (2016a). Chemical composition and source apportionment of ambient $PM_{2.5}$ during the non-heating period in Taian, China. *Atmos. Res.* 170: 23–33.

Liu, D., Niu, S., Yang, J., Zhao, L., Lü, J. and Lu, C. (2012). Summary of a 4-year fog field study in Northern Nanjing, Part 1: Fog boundary layer. *Pure Appl. Geophys.* 169: 809–819.

Liu, Q., Baumgartner, J., Zhang, Y. and Schauer, J.J. (2016b). Source apportionment of Beijing air pollution during a severe winter haze event and associated pro-inflammatory responses in lung epithelial cells. *Atmos. Environ.* 126: 28–35.

Liu, Z., Hu, B., Zhang, J., Yu, Y. and Wang, Y. (2016c). Characteristics of aerosol size distributions and chemical compositions during wintertime pollution episodes in Beijing. *Atmos. Res.* 168: 1–12.

Ma, L., Li, M., Zhang, H., Li, L., Huang, Z., Gao, W., Chen, D.H., Fu, Z., Nian, H.Q., Zou, L.L., Gao, J., Chai, F.H. and Zhou, Z. (2016). Comparative analysis of chemical composition and sources of aerosol particles in urban Beijing during clear, hazy, and dusty days using single particle aerosol mass spectrometry. *J. Cleaner Prod.* 112: 1319–1329.

Meng, C.C., Wang, L.T., Zhang, F.F., Wei, Z., Ma, S.M., Ma, X. and Yang, J. (2016). Characteristics of concentrations and water-soluble inorganic ions in $PM_{2.5}$ in Handan City, Hebei province, China. *Atmos. Res.* 171: 133–146.

Ohta, S. and Okita, T. (1990). A chemical characterization of atmospheric aerosol in Sapporo. *Atmos. Environ.* 24: 815–822.

Pathak, R.K., Wu, W.S. and Wang, T. (2009). Summertime $PM_{2.5}$ ionic species in four major cities of China: Nitrate formation in an ammonia-deficient atmosphere. *Atmos. Chem. Phys.* 9: 1711–1722.

Peng, H.Q, Liu, D.Y., Zhu, B., Su, Y., Wu, J.M., Shen, H., Wei, J.S. and Cao, L. (2016). Boundary-layer characteristics of persistent regional haze events and heavy haze days in Eastern China. *Adv. Mete.* 2016: 6950154.

Pierson, W.R., Brachaczek, W.W. and McKee, D.E. (1979). Sulfate emissions from catalyst-equipped automobiles on the highway. *J. Air Pollut. Control Assoc.* 29: 255–257.

Qian, W.H., Zhu, J., Wang, Y.G. and Fu, J.L. (2009). Regional relationship between the Jiang-Huai Meiyu and the equatorial surface-subsurface temperature anomalies. *Chin. Sci. Bull.* 54: 113–119.

Ram, K., Sarin, M.M. and Tripathi, S.N. (2012). Temporal trends in atmospheric $PM_{2.5}$, $PM_{10}$, elemental carbon, organic carbon, water-soluble organic carbon, and optical properties: Impact of biomass burning emissions in the Indo-Gangetic Plain. *Environ. Sci. Technol*. 46: 686–695.

Shi, H., Wang, Y., Chen, J. and Huisingh, D. (2016). Preventing smog crises in China and globally. *J. Cleaner Prod.* 112: 1261–1271.

Su, J., Zhao, P. and Dong, Q. (2018). Chemical compositions and liquid water content of size-resolved aerosol in Beijing. *Aerosol Air Qual. Res.* 18: 680–692.

Sun, Y., Jiang, Q., Xu, Y., Ma, Y., Zhang, Y., Liu, X., Li, W., Wang, F., Li, J., Wang, P. and Li, Z. (2016). Aerosol characterization over the North China Plain: Haze life cycle and biomass burning impacts in summer. *J. Geophys. Res.* 121: 2508–2521.

Tan, J., Duan, J., Zhen, N., He, K. and Hao, J. (2016). Chemical characteristics and source of size-fractionated atmospheric particle in haze episode in Beijing. *Atmos. Res.* 167: 24–33.

Tröstl, J., Chuang, W.K., Gordon, H., Heinritzi, M., Yan, C., Molteni, U., Ahlm, L., Frege, C., Bianchi, F., Wagner, R., Simon, M., Lehtipalo, K., Williamson, C., Craven, J.S., Duplissy, J., Adamov, A., Almeida, J., Bernhammer, A.K., Breitenlechner, M., Brilke, S., Dias, A., Ehrhart, S., Flagan, R.C., Franchin, A., Fuchs, C., Guida, R., Gysel, M., Hansel, A., Hoyle, C.R., Jokinen, T., Junninen, H., Kangasluoma, J., Keskinen, H., Kim, J., Krapf, M., Kürten, A., Laaksonen, A., Lawler, M.,

Leiminger, M., Mathot, S., Möhler, O., Nieminen, T., Onnela, A., Petäjä, T., Piel, F.M., Miettinen, P., Rissanen, M.P., Rondo, L., Sarnela, N., Schobesberger, S., Sengupta, K., Sipilä, M., Smith, J.N., Steiner, G., Tomè, A., Virtanen, A., Wagner, A.C., Weingartner, E., Wimmer, D., Winkler, P.M., Ye, P., Carslaw, K.S., Curtius, J., Dommen, J., Kirkby, J., Kulmala, M., Riipinen, I., Worsnop, D.R., Donahue, N.M. and Baltensperger, U., (2016). The role of low-volatility organic compounds in initial particle growth in the atmosphere. *Nature* 533: 527–531.

Truex, T.J., Pierson, W.R. and McKee, D.E. (1980). Sulfate in diesel exhaust. *Environ. Sci. Technol.* 14: 1118–1121.

Wang, H., Zhu, B., Shen, L., Xu, H., An, J., Xue, G. and Cao, J. (2015). Water-soluble ions in atmospheric aerosols measured in five sites in the Yangtze River Delta, China: Size-fractionated, seasonal variations and sources. *Atmos. Environ.* 123: 370–379.

Wang, H.L., Zhu, B., Shen, L. and Kang, H.Q. (2012a). Size distributions of aerosol and water-soluble ions in Nanjing during a crop residual burning event. *J. Environ. Sci.* 24: 1457–1465.

Wang, T., Jiang, F., Deng, J., Shen, Y., Fu, Q., Wang, Q., Fu, Y., Xu, J. and Zhang, D. (2012b). Urban air quality and regional haze weather forecast for Yangtze River Delta region. *Atmos. Environ.* 58: 70–83.

Wang, H.L., Qiao, L.P., Lou, S.R., Zhou, M., Ding, A.J., Huang, H.Y., Chen, J.M., Wang, Q., Tao, S.K., Chen, C.H., Li, L. and Huang, C. (2016). Chemical composition of $PM_{2.5}$ and meteorological impact among three years in urban Shanghai, China. *J. Cleaner Prod.* 112: 1302–1311.

Wang, X., Ye, X., Chen, H., Chen, J., Yang, X. and Gross, D.S. (2014). Online hygroscopicity and chemical measurement of urban aerosol in Shanghai, China. *Atmos. Environ.* 95: 318–326.

Wang, Y., Zhuang, G., Tang, A., Yuan, H., Sun, Y., Chen, S. and Zheng, A. (2005). The Ion Chemistry and the Source of $PM_{2.5}$ Aerosol in Beijing. *Atmos. Environ.* 39: 3771–3784.

Wen, B., Kong, S.F., Yin, Y., Chen, K., Yuan, L., Li, L. and Li, Q. (2014). Size distribution of water-soluble ions in aerosol from an offshore site of Nantong in autumn. *China Environ. Sci.* 34: 49–57. (in Chinese)

Wen, B., Yin, Y., Qin, Y.S. and Chen, K. (2013). Chemical characteristics of water-soluble components of aerosol particles at different altitude of the Mount Huang in the Summer. *Environ. Sci.* 34: 1973–1981. (in Chinese)

Xu, H., Cao, J., Chow, J.C., Huang, R.J., Shen, Z., Chen, L.W.A., Ho, K.F. and Watson J.G. (2016). Inter-annual variability of wintertime $PM_{2.5}$ chemical compositions in Xi'an, China: Evidences of changing source emissions. *Sci. Total Environ.* 545: 546–555.

Yan, C., Zheng, M., Sullivan, A.P., Bosch, C., Desyaterik, Y., Andersson, A., Li, X., Guo, X., Zhou, T., Gustafsson, Ö. and Collett, J.L. (2015). Chemical characteristics and light-absorbing property of water-soluble organic carbon in Beijing: Biomass burning contributions. *Atmos. Environ.* 121: 4–12.

Yang, J., Xie, Y.J., Shi, C.E., Liu, D.Y., Niu, S.J. and Li, Z.H. (2012). Ion composition of fog water and its relation to air pollutants during winter fog events in Nanjing, China. *Pure Appl. Geophys.* 169: 1037–1052.

Yang, Y., Zhou, R., Wu, J., Yu, Y., Ma, Z., Zhang, L. and Di, Y. (2015). Seasonal variations and size distributions of water-soluble ions in atmospheric aerosols in Beijing, 2012. *J. Environ. Sci.* 34: 197–205.

Yao, X., Chan, C.K., Fang, M., Cadle, S., Chan, T., Mulawa, P., He, K. and Ye, B. (2002). The water-soluble ionic composition of $PM_{2.5}$ in Shanghai and Beijing, China. *Atmos. Environ.* 36: 4223–4234.

Zhang, Y., Shao, M., Lin, Y., Luan, S., Mao, N., Chen, W. and Wang, M. (2013). Emission inventory of carbonaceous pollutants from biomass burning in the Pearl River Delta Region, China. *Atmos. Environ.* 76: 189–199.

Zhao, M., Huang, Z., Qiao, T., Zhang, Y., Xiu, G. and Yu, J. (2015). Chemical characterization, the transport pathways and potential sources of $PM_{2.5}$ in Shanghai: Seasonal variations. *Atmos. Res.* 158/159: 66–78.

Zhao, X., Wang, X., Ding, X., He, Q., Zhang, Z., Liu, T., Fu, X., Gao, B., Wang, Y., Zhang, Y., Deng, X. and Wu, D. (2014). Compositions and sources of organic acids in fine particles ($PM_{2.5}$) over the Pearl River Delta region, south China. *J. Environ. Sci.* 26: 110–121.

Zhou, X., Cao, Z., Ma, Y., Wang, L., Wu, R. and Wang, W. (2016). Concentrations, correlations and chemical species of $PM_{2.5}/PM_{10}$ based on published data in China: Potential implications for the revised particulate standard. *Chemosphere* 144: 518–526.

Zhou, Y.Y., Ma, Y., Zheng, J., Cui, F.P. and Wang, L. (2015). Pollution characteristics and light extinction effects of water-soluble ions in $PM_{2.5}$ during winter haze days at North suburban Nanjing. *Environ. Sci.* 36: 1926–1934. (in Chinese)

*Received for review, April 25, 2018*
*Revised, August 10, 2018*
*Accepted, August 12, 2018*